Nickel atom and ion densities in an inductively coupled plasma with an internal coil

Lin Xu[a)]
*Plasma Processing Laboratory, Department of Chemical and Biomolecular Engineering,
University of Houston, Houston, Texas 77204-4004*

Nader Sadeghi[b)]
*Laboratoire de Spectrométrie Physique, University Joseph Fourier-Grenoble and CNRS,
38042, Grenoble, France*

Vincent M. Donnelly[c)] and Demetre J. Economou[d)]
*Plasma Processing Laboratory, Department of Chemical and Biomolecular Engineering,
University of Houston, Houston, Texas 77204-4004*

The nickel atom density was measured in an inductively coupled argon plasma with an internal Ni coil, as a function of pressure and power, using optical absorption spectroscopy. Nickel atoms were sputtered from the coil and from a separate Ni target under optional target bias. A fraction of the atoms was ionized in the high-density plasma. The gas temperature was determined by analyzing the rovibrational spectra of the second positive system of nitrogen actinometer gas. The electron density was determined by optical emission spectroscopy in combination with a global model. For a pressure of $8-20$ mTorr and coil power of $40-200$ W, the Ni atom density ranged from 2.7×10^9 to 1.5×10^{10} cm^{-3}, increasing strongly with pressure. The Ni atom density first increased with power but saturated at high power levels. The measured Ni atom density agreed fairly well with the predictions of a global model, in particular, at the higher pressures. The model also predicted that the Ni$^+$ ion density greatly increased at higher powers and pressures. Applying 70 W bias on the target electrode increased the Ni atom density by 60%. © *2007 American Institute of Physics.* [DOI: 10.1063/1.2401659]

I. INTRODUCTION

Ionized physical vapor deposition (IPVD) remains a viable method for future applications in barriers for tungsten wiring and for copper seed layers.[1] In the IPVD process, a radio frequency (rf) high-density inductively coupled plasma (ICP) is created in an inert gas (e.g., argon), usually by immersing the ICP coil in the plasma. Metal atoms are sputtered from a separately rf-powered target. These sputtered atoms are ionized as they traverse the plasma, and the ions gain directionality in the sheath over the biased substrate, causing anisotropic filling of high-aspect-ratio trenches.[2,3] When the coil is made of the metal of interest and is directly exposed to the plasma, as in the present work, it can serve as an additional source of sputtered atoms.

In addition to IPVD, this system can be used to extract a high-flux metal ion beam for other metal deposition applications. One such process that we have recently reported, nanopantography, is a method for creating nanosize patterns in a massively parallel fashion over large areas.[4] A monoenergetic, collimated ion beam is extracted from a plasma[5] and encounters a substrate in a downstream high vacuum chamber. Ion beamlets are focused on the substrate by electrostatic lenses built on the substrate using standard photolithography

and etching. An inert gas ion beam may be used in combination with chlorine gas to etch nanoholes in silicon at the focal points of the beamlets. Nanopantography can result in size reduction of 100 times, i.e., a 1000 nm diameter lens can produce a 10 nm diameter hole.[4] When using a metal ion beam without any added gas, nanopantography can deposit nanosize metal islands. These in turn could serve as catalysts for the growth of carbon nanotubes.[6,7] Although some control over the diameter and spacing of catalyst dots has been realized by photolithography,[8] large-area fabrication of uniform, location-specific sub-10 nm catalyst dots, which is critical for the synthesis of isolated single-wall carbon nanotubes (SWCNTs), is still extremely difficult. Nanopantography has the potential of producing sub-10 nm Ni dots in well-defined positions over large areas, which will potentially open a route for the massive production of prespecified patterns of SWCNTs. The generation of a metal (e.g., nickel) ion beam is critical for this and other applications.

To extract a high flux of monoenergetic, collimated nickel ions, the density of Ni species (atoms and ions) in the plasma and their dependence on operating conditions are of primary importance. Common diagnostics to monitor or measure the density of metal species in a metal-containing plasma include quartz crystal microbalance (QCM) with ion-repelling grids,[9] cross sectional scanning electron microscopy (SEM) of high-aspect-ratio test features,[10] optical emission spectroscopy (OES),[11] and optical absorption spectroscopy (OAS).[12,13] OES and OAS are attractive be-

a)Electronic mail: lxu3@mail.uh.edu
b)Electronic mail: sadeghi@ujf-grenoble.fr
c)Electronic mail: vmdonnelly@uh.edu
d)Electronic mail: economou@uh.edu
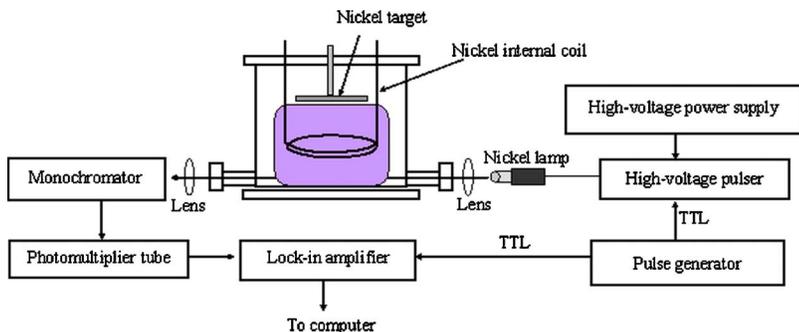
FIG. 1. (Color online) Schematic of the plasma chamber and optical diagnostic setup.

cause they are nonintrusive and relatively easy to set up. OES can provide qualitative information on the densities of various species in the discharge; while OAS can provide the absolute number density if a resonant absorption line with strong oscillator strength for the species of interest can be identified. For the estimate of argon density, the gas temperature (T_g) should be known because, at fixed pressure, the neutral density is inversely proportional to T_g. Interpretation of absorption measurements requires the value of T_g as well. In this work, Ni neutral densities were measured by OAS, during sputtering of Ni in an argon ICP with the Ni coil and Ni target immersed in the plasma. T_g was determined by OES from the rotational temperature of trace added N_2, and relative electron densities were derived from the OES of Ar. Finally, Ni neutral and ion densities were computed from a global model.

II. EXPERIMENTAL APPARATUS

A schematic of the experimental setup is shown in Fig. 1. The reactor was a 6 in. diameter 8 in. high stainless steel cylinder. A 3.5 in. outside diameter (o.d.) two-turn (total height of 1.5 in.) water-cooled antenna coil, fabricated from $\frac{1}{4}$ in. o.d. nickel tubing (99.0% purity), was suspended 2.3 in. above the bottom of the reactor. 13.56 MHz radio-frequency (rf) power was delivered through a matching network to the induction coil. A 3 in. diameter nickel target disk (99.98% pure), 0.7 in. above the top of the coil, could be negatively biased by a 12.56 MHz rf power through a matching network. Power was measured with in-line Bird meters. The voltages on the coil (high-voltage end) and on the target were measured with a 100 times high-voltage probe. The discharge gas was 99.999% pure argon at a flow rate of 20 SCCM (SCCM denotes cubic centimeter per minute at STP), at pressures of 8–20 mTorr.

The light source for absorption spectroscopy was a Ni hollow cathode lamp filled with Ne gas. This lamp was pulsed by a high-voltage pulser at 100 Hz and 50% duty cycle (5 ms on/5 ms off) controlled by a pulse generator. The discharge current was set at 15 mA during the pulse-on period by tuning the voltage output from a high-voltage power supply. The common axis of the two optical diagnostic quartz windows was located 1.5 in. below the bottom end of the coil (Fig. 1). The window transmittance was about 90% in the range of 300–1000 nm and was ~60% at 232.0 nm used in the Ni atom optical absorption. The windows were isolated with gate valves when no optical diagnostic experiments were performed, to avoid metal deposition on the win-

dows, which would attenuate their transmission. The source lamp was located at the focal point of a quartz lens, to provide a parallel beam through the plasma, while another quartz lens focused the transmitted light onto the entrance slit of a single monochromator (Jobin-Yvon U1000) equipped with a GaAs photomultiplier tube (PMT, Hamamatsu R955). The monochromator had a grating with 2400 grooves/mm and 1000 mm focal length. The resolution was ~0.5 Å full width at half maximum (FWHM) with slit widths of 130 μm. For OES measurements, the PMT signal was collected directly and processed by LABVIEW™. For absorption measurements, a lock-in amplifier (SR 530, Stanford Research Systems), triggered by the same pulse used for the lamp, processed the PMT signal to record the time-modulated signal at a chosen absorption line. The same setup was used to record spectra of optical emission induced by the plasma. OES was used to determine relative electron densities and gas temperatures (with traces of added N_2).

III. RESULTS AND DISCUSSION

The main goals of this study were to determine the absolute Ni atom and ion number densities and determine the optimum conditions for extracting a monoenergetic Ni$^+$ beam from a pulsed ICP. We now present measurements and computations to obtain these goals.

A. Gas temperature measurements

The gas temperature (T_g) determines the number densities of Ar or Ni atoms in the plasma, at a fixed pressure, by the ideal gas law. T_g is also needed for measurement of Ni number densities using optical absorption spectroscopy, as described below. One method for obtaining T_g is to add a small quantity of N_2 to the gas and obtain the rotational temperature (T_r) of $N_2(C\,^3\Pi_u)$ from a fit of the N_2 second positive ($C\,^3\Pi_u$-$B\,^3\Pi_g$) plasma-induced emission spectra.[14–17] The rotational population distribution of $N_2(C\,^3\Pi_u)$ reflects the rotational temperature of the $N_2(X\,^1\Sigma_u)$ ground state molecules, since the ~40 ns radiative lifetime of the C state is too short to permit collisional rotational redistribution within this state and the rotational angular momentum J is conserved during electron impact excitation of the C state from the ground state $X\,^1\Sigma_u$.

In equating T_r with T_g in the presence of added N_2, several requirements must be satisfied. First, any perturbation of the plasma by adding N_2 should be small. In our case, with 2% added N_2, the Ar emission at 750.4 nm was attenu-

ated by only ∼10%, indicating an acceptably small degree of perturbation. Next, the bath gas (e.g., Ar) and N_2 must be in thermal equilibrium. At the lowest pressure of 8 mTorr, the mean free path (mfp) for elastic collisions between neutrals is about 1 cm, much smaller than the ∼10 cm reactor dimensions. Similarly, the cross section for rotational energy transfer is ∼10^{-14} cm²,[18,19] yielding a collision frequency of ∼10^5 s^{-1} at 10 mTorr and a mfp of ∼1 cm for this process. The N_2 mfp for rotational excitation collisions with electrons is about 10 cm for an electron density, $n_e = 10^{11}$ cm^{-3}, and an electron temperature of 3 eV (collision frequency ∼10^4 s^{-1});[20] hence rotational heating of N_2 by collisions with electrons is minimized.

The strong 0-0 band of the second positive system at 337.1 nm is usually chosen to probe the rotational distribution of the C state. However, in most Ar plasmas, especially at lower electron densities, the N_2 $C(0-0)$ band is preferentially excited by Ar metastables.[21–24] Figure 11 of Ref. 25 shows that, at room temperature, the most abundant $Ar^*(^3P_2)$ ($1s_5$ in Paschen's notation) metastable atoms populate the $v = 0$, 1, and 2 levels of the C state, while the 0.15 eV higher lying $Ar^*(^3P_0)$ ($1s_3$ in Paschen's notation) metastables populate levels up to $v=3$. The density of $Ar^*(1s_3)$ atoms is typically ∼10 times smaller than that of $Ar^*(1s_5)$ and the rate coefficient for population of the $C(v=3)$ state by $Ar^*(1s_3)$ is 20 times smaller than that for production of the $C(v=0)$ state by $Ar^*(1s_5)$.[25] Consequently, electron impact excitation usually dominates energy transfer from Ar^* metastables for populating the $v=3$, and obviously $v=4$, levels of the C state. Thus the 3-3 and 4-4 bands (heads at 328.5 and 326.8 nm, respectively) provided reasonable values for T_g under all conditions in most Ar plasmas.

Sample spectra of N_2 second positive bands are presented in Fig. 2. For transitions originating from $v=0$ level of the C state, to account for the energy transfer from Ar^* metastables, the 0-0 band was fitted assuming a two-temperature rotational distribution according to

$$[N_J] \propto (2J+1)\left[\exp(-F_J/kT_r^L) + \varphi\frac{T_r^L}{T_r^H}\exp(-F_J/kT_r^H)\right], \quad (1)$$

where $[N_J]$ is the density of the J rotational level, F_J is its energy, T_r^L and T_r^H are temperatures of two Boltzmann distributions, and φ is the ratio of total populations for these two distributions. T_r^L and T_r^H would correspond to distributions originating from electron impact excitation from the ground state and to energy transfer from Ar^* metastables, respectively. In fact, considering the pressure range examined, the rotational transfer frequency ($\leq 5 \times 10^5$ s^{-1}) is much smaller than the radiative decay frequency (2.6×10^7 s^{-1}) of the C state, and hence population by these two mechanisms can be distinguished. In Fig. 2, the overpopulation of high rotational levels is clearly seen. The best fit of experimental data was obtained with $T_r^L = 360$ K and $T_r^H = 2000$ K. The minor misfit at 338 nm is due to contribution from the 1-1 band that was not included in the fit. The T_r^H value is very similar to that found in afterglow experiments where N_2 was exclusively populated by energy transfer from Ar^* metastables.[21,22] The 3-3 and 4-4 bands were fitted to a single T_r. These bands are
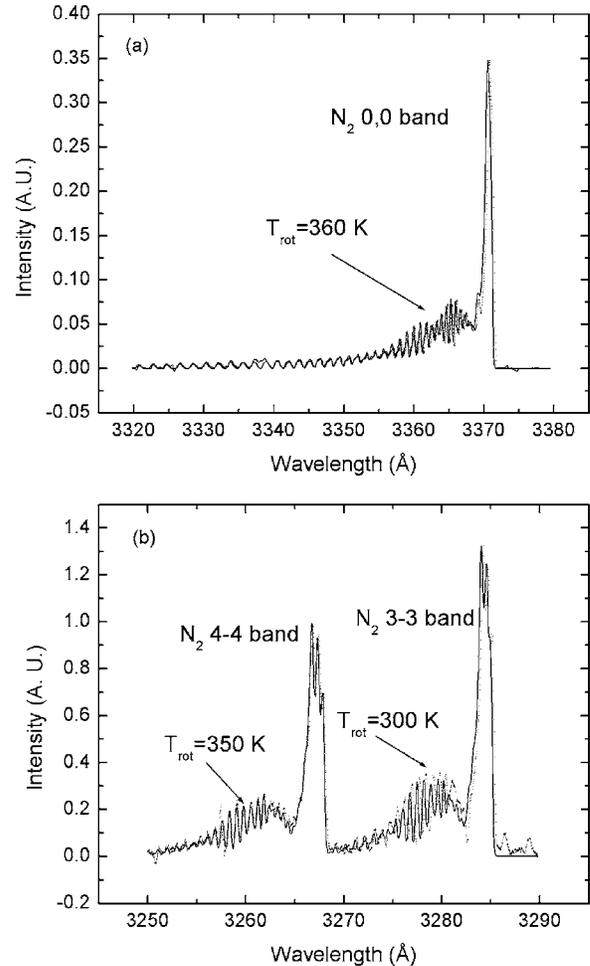
FIG. 2. Example emission spectra of $N_2(C\,^3\Pi_u - B\,^3\Pi_g)$ at 40 W, 8 mTorr, 2% N_2 in the Ar feed gas: (a) 0-0 band and (b) 3-3 plus 4-4 bands. Experimental points and the solid line fit to the spectra are shown.

slightly overlapping and hence have been fitted together. The quality of the fit for the 3-3 band is degraded somewhat because this band is spoiled by the tail of 0-0 and 2-2 (head at 330.9 nm) bands.

Table I presents temperatures at the four extreme conditions in this study. The 0-0 and 4-4 bands yield very similar values under all conditions. T_r deduced from the 3-3 band is not as reliable; it is lower, especially at 8 mTorr. Besides the interfering overlap with the 0-0 and 2-2 bands mentioned above, the smaller T_r of the 3-3 band can also be explained

TABLE I. Rotational temperatures T_r, determined from the best fit of nitrogen $\Delta v = 0$ bands, in an Ar plasma containing 2% N_2, gas temperatures T_g, derived from the average of these values (excluding the 3-3 values at 8 mTorr—see text), and electron temperatures T_e, computed from a global model.

Plasma condition		T_r (K)				
Power (W)	Pressure (mTorr)	0-0	3-3	4-4	T_g (K)	T_e (eV)
40	20	350	350	370	360±20	2.19
200	20	450	420	480	450±30	2.30
40	8	360	300	350	355±20	2.53
200	8	440	350	470	455±20	2.62

by the fact that $v=3$ of the C-state is partially populated by energy transfer from $Ar^*(1s_3)$ atoms,[25] but the limited available energy populates mostly the low rotational levels. The next to last column of Table I gives our best estimates for T_g, using the average of the 0-0, 3-3, and 4-4 values at 20 mTorr and the average of the 0-0 and 4-4 band values at 8 mTorr. At fixed ICP power, no appreciable temperature change was observed between 8 and 20 mTorr pressures. An ~100 K rise in the T_g was found when the ICP power increased from 40 to 200 W at either pressure. Since T_g values were rather low, and the ±20 K accuracy is insufficient to capture more subtle details of variations with power and pressure, T_g was linearly interpolated for other experimental conditions.

B. Calculation of electron temperature

The electron temperature (T_e) was estimated from a global model,[26] including ionization of Ar metastables. Thus, by rearranging the Ar^+ mass balance one obtains

$$\frac{k_{iz}(T_e)n_g + k_{iz}^*(T_e)n_{Ar^*}}{u_B(T_e)} = \frac{1}{d_{eff}}, \tag{2}$$

with the effective plasma length d_{eff} given by

$$d_{eff} = \frac{1}{2}\frac{RL}{Rh_L + Lh_R}, \tag{3}$$

where k_{iz} and k_{iz}^* are ionization rate coefficients from ground state or metastable state, respectively. n_{Ar^*}, u_B, R, L, h_R, and h_L are metastable Ar density, Bohm velocity of argon ions, radius, and length of the cylindrical plasma, and ratios of plasma density at the radial and axial sheath edges to that at the plasma center, respectively. k_{iz}^* was calculated based on the ionization cross section of argon metastables ($1s_5$ in Paschen's notation) provided by McGuire.[27] Given $k_{iz}=2.3 \times 10^{-8}T_e^{0.68}\exp(-15.76/T_e)$ cm^3 s^{-1},[28] $h_R=0.18-0.26$ and $h_L=0.17-0.25$, for the chosen experimental conditions, and $n_g(\text{cm}^{-3})=3.3\times10^{13}p(298/T_g)$, with pressure p in mTorr, T_e can be expressed as a function of metastable Ar density n_{Ar^*}. The number densities of argon metastables $1s_5$ and $1s_3$ were lumped into n_{Ar^*}, resulting in a mass balance of Ar^*,

$$k_{ex}^*(T_e)n_e n_g = \left\{[k_q^*(T_e) + k_{iz}^*(T_e)]n_e + \frac{D_{Ar^*}}{\Lambda^2}\right\}n_{Ar^*}, \tag{4}$$

where k_{ex}^*, k_q^*, n_e, D_{Ar^*}, and Λ are the Ar^* excitation rate constant from the Ar ground state, Ar^* quenching rate constant by electrons, electron density, diffusion coefficient of Ar^* in argon gas, and characteristic diffusion length of Ar^*. $k_{ex}^*=3.71\times10^{-8}\exp(-15.06/T_e)$ cm^3 s^{-1} and $k_q^*\approx2\times10^{-7}$ cm^{-3} s^{-1}.[29] $D_{Ar^*}=2.42\times10^{18}/n_g$ cm^2/s was taken from Lymberopoulos and Economou.[30] The electron density n_e was estimated from an energy balance and will be described in detail in the next section. Λ is the characteristic diffusion length of a cylindrical chamber of length L (11.4 cm) and radius R (7.6 cm),

$$\frac{1}{\Lambda^2} = \left(\frac{\pi}{L}\right)^2 + \left(\frac{2.405}{R}\right)^2, \tag{5}$$

hence $\Lambda=2.4$ cm. By solving Eqs. (3) and (4) numerically, n_{Ar^*} and T_e were obtained for each plasma condition (Table I). It was found that with Ar^* species included in Eq. (2) the calculated T_e was $0.1-0.2$ eV lower than that obtained without considering the Ar^* species. The Ar^* density was in the range of $(3.5-5.5)\times10^{10}$ cm^{-3} with a weak dependence on pressure and power. The ratio of argon metastable density to ground state density was in the range of $(1-3)\times10^{-4}$, similar to the ratios in an Ar/Cl_2 plasma with the same T_e.[31] The electron temperature of Table I increases with power at a given pressure, due to gas heating which results in lower gas number density as power increases.

C. Determination of electron density using optical emission spectroscopy and a power balance

For excited states of Ar that are produced predominantly by electron impact from the ground state (and not from the metastable states), the intensity of emission from the excited state is

$$I_{g,x} = ak_{g,x}n_g n_e, \tag{6}$$

where a is a proportionality constant, $k_{g,x}$ is a rate coefficient that depends on the electron energy distribution function (EEDF), and n_e is the electron number density. Assuming a Maxwellian EEDF described by T_e, relative n_e can be determined from the emission intensity and $n_g=3.3\times10^{13}p(298/T_g)$, if the dependence of $k_{g,x}$ on T_e is known. The Ar emission line at 419.8 nm $(3s^23p^5(^2P_{3/2}^0)5p -3s^23p^5(^2P_{3/2}^0)4s$, also notated as $3p_5-1s_4$ in Paschen's or $5p[1/2]_0-4s[3/2]_1^0$ in Racah's notations) was chosen because the excited state ($3p_5$) of this transition was expected to be populated primarily by electron impact excitation from the ground state and the cross section is known.[32] Strong contributions to the emission intensity through electron impact excitation from metastables are less likely. This can be explained by noting that the upper state of the transition ($3p_5$) has $J=0$ and optical transitions to metastable states $1s_5$ or $1s_3$, with $J=2$ or 0, are forbidden. For such an optically forbidden transition, excitation through electron impact is unlikely. For example, the measured electron impact excitation cross section to this state from Ar metastable $1s_5$ or $1s_3$ to $2p_1$ ($J=0$) or $2p_5$ ($J=0$) is much smaller than to the other optically allowed states having $J=1$, 2, or 3.[33,34]

Since a pulsed plasma is used for monoenergetic ion beam extraction in nanopantography,[4,5] OES measurements were taken in an Ar plasma modulated at 5 kHz and 50% duty cycle (100 μs pulse on and 100 μs pulse off). Simulations[35,36] and experiments[37] in pulsed inductively coupled Ar plasmas have shown that the plasma evolves into a quasi-steady-state ~10 μs after the pulse-on time. Therefore, the emission intensity of an Ar line recorded in the pulsed plasma should be comparable to that in a continuous-wave plasma with double the average power used in the pulsed plasma. Since we only use these measurements for relative estimates of electron density, this distinction is largely irrelevant.
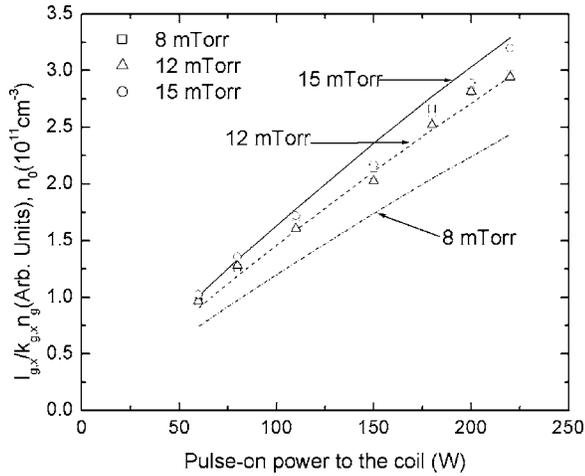
FIG. 3. Relative electron number density determined from the optical emission intensity of Ar 419.8 nm line (symbols), divided by Ar number density (and corrected for a small increase in the excitation rate due to an increase in T_e), as a function of pulse-on power to the internal coil. The plasma was pulsed at 5 kHz and 50% duty cycle, and there was no power on the target. The solid lines represent absolute electron densities derived from a model of a continuous-wave plasma with power identical to that during the power-on fraction of the cycle of the pulsed plasma. The measurements have been normalized to the calculations at 12 mTorr and 220 W.

The relative n_e computed from Ar emission intensities, Eq. (6) and T_e values computed above (Table I), is plotted in Fig. 3 as a function of pulse-on power to the coil (double the measured average power) at 8, 12, and 15 mTorr. The relative n_e increases almost linearly with power, with no abrupt jump in emission with increasing power that would indicate a capacitive-to-inductive mode transition.[38] This suggests that the plasma was operated predominantly in an inductively coupled mode throughout the power range investigated.

The absolute electron density in a continuous-wave plasma was also estimated by an energy balance,[26]

$$n_0 = \frac{P_{abs}}{eu_B A_{eff} \varepsilon_T},$$

(7)

where

$$A_{eff} = 2\pi R(Rh_L + Lh_R).$$

(8)

P_{abs} is the power absorbed by the plasma, assumed to be 80% of the total input power, and ε_T is the total energy loss per electron-ion pair formed. The power and pressure dependence of the relative electron densities derived from Ar emission are in good agreement with the absolute electron densities derived from the energy balance (lines in Fig. 3).

The effect of target power on the Ar emission intensity at 419.8 nm and hence n_e was also examined. The Ar emission intensity remained unchanged for target power values up to 100 W, indicating that the plasma is mainly sustained by the internal coil. Also, it appears that additional nickel sputtered from the target was not enough to modify the plasma density and/or electron temperature.

D. Nickel atom number density

1. Optical absorption measurements

A description of the resonant absorption techniques can be found elsewhere.[12,13,39] The fractional absorption, $A_L = (I_0 - I)/I_0$, where I_0 and I are the transmitted line intensities without and with plasma, respectively, is given by

$$A_L = \sum_{m=1}^{\infty} -\frac{(-k_0 l)^m}{m!\sqrt{1+m\alpha^2}},$$

(9)

where l is the absorption length, α is the ratio of emission (i.e. lamp)-to-absorption linewidths, and k_0, the absorption coefficient in units of cm^{-1} at the center of the line, is given by

$$k_0 = \frac{8.25 \times 10^{-13} f}{\Delta\sigma^A}\langle[Ni]\rangle,$$

(10)

where f is the oscillator strength, $\Delta\sigma^A$ is the absorption linewidth, and $\langle[Ni]\rangle$ is the absorption line-of-sight average density of nickel atoms (cm^{-3}). Assuming that Stark and pressure broadening are negligible in both the lamp (emitter) and the plasma (absorber), the line profiles are Doppler shaped, with linewidths (FWHM) $\Delta\sigma$ given by

$$\Delta\sigma = 7.16 \times 10^{-7} \sigma \sqrt{\frac{T}{M}},$$

(11)

where $\sigma = (10^7/\lambda)$ and $\Delta\sigma$ are in units of (cm^{-1}), λ is the wavelength of the transition in nm, T is the temperature of either the emitter or absorber in K, and the atomic mass $M = 59$ for nickel. Using the definition of α and Eq. (11) one obtains

$$\alpha^2 = (T^E/T^A),$$

(12)

where T^E is the gas temperature in the lamp [~ 600 K at the lamp discharge current of 15 mA (Ref. 40)] and T^A is the absorbing species temperature in the plasma (equal to the gas temperature, which ranges from 360 to 455 K for the conditions investigated—see Table I).

To determine the ground state $3d^8 4s^2$ ($a^3 F_4$) Ni atom density, the 232.0 nm line was chosen with transition probability $A = 6.9 \times 10^8$ s^{-1} corresponding to an oscillator strength $f = 0.68$. This line has the largest f value of all Ni lines ending in the ground state fine-structure levels. Thus, it provides the largest absorption. The Doppler width for this Ni line is

$$\Delta\sigma_{232} = 0.00402(T_g)^{1/2}.$$

(13)

Since $\langle[Ni]_{J=4}\rangle$ depends on absorption in a nonlinear fashion, it is much easier to calculate a set of absorption rates for different $\langle[Ni]_{J=4}\rangle$ densities [only the first two terms in Eq. (9) were retained] and then deduce $\langle[Ni]_{J=4}\rangle$ by comparing the measured A_L absorption values to the calculated one.

The ground electronic state configuration has additional $J=3$ and 2 sublevels, located at 1332 and 2216 cm^{-1} above the $J=4$ sublevel, as well as a $3d^9 4s$ ($a^3 D$) metastable state, with $J=3$, 2, and 1 sublevels at 205, 880, and 1713 cm^{-1}, respectively. Therefore the total Ni density is the sum of the populations of these six low lying levels, and the measured

density must be multiplied by a factor, between 1 (if all Ni is only in the $a\,^3F_4$ ground state) and $(36/9)=4$ (the sum over $2J+1$ statistical weights, with equal Boltzmann factors for all levels) to obtain the true Ni number density.

The population partition of Ni atoms ejected from a target after Ar$^+$ ion bombardment in the keV range has been investigated.[41–44] A striking result was the pronounced population inversion of $a\,^3D_3$ and $a\,^3D_2$ sublevels in Ni metastable state, with respect to the electronic ground state. The density ratio $a\,^3F_4 : a\,^3D_3 : a\,^3D_2$ should be close to 9:7:5 with equal Boltzmann factors. However, the measured populations of $a\,^3D_3$ and $a\,^3D_2$ were 60% more than that of the ground state $3d^84s^2$ ($a\,^3F_4$) during sputtering of polycrystalline Ni target by Ar$^+$ ions with energies 3–12 keV.[44] More surprisingly, for a single crystal Ni (001) target under bombardment by 5 keV Ar$^+$ ions, the populations of $a\,^3D_3$ and $a\,^3D_2$ were found to be 5.7 and 7.4 times that of $a\,^3F_4$, respectively.[43] This remarkable disparity in the Ni partition factor could originate either from target crystal structure differences or from differences in experimental techniques.[42,44] In our study, the coil and target were polycrystalline Ni, and the ion sputtering energies were ~100 eV on the coil and several hundreds of eV on the Ni target with the power ranging from 40 to 70 W. The energy dependence of low ion-energy Ar$^+$ bombardment on the population distributions of sputtered Ni atoms has not been reported; however, we expect that at this lower ion energy, a smaller fraction of Ni metastables could be produced. We therefore assumed that the populations of Ni $a\,^3F$ and $a\,^3D$ manifolds ejected from the coil and/or target follow their statistical weights.

When sputtered Ni atoms traverse the plasma, subsequent collisions of Ni atoms with electrons ($T_e \approx 2.4$ eV) would preserve this distribution or even produce more metastable-state Ni atoms by electron impact excitation,[45] whereas collisions with Ar atoms ($T_g \approx 0.04$ eV ≈ 300 cm^{-1}) would cool the distribution.[46,47] In fact, the population transfer between the $a\,^3D$ ($3d^94s^1$ configuration) and $a\,^3F$ ($3d^84s^2$ configuration) manifolds by collision with Ar atoms in the plasma is expected to be very small because rare-gas collisions are very inefficient for transferring an electron from a $3d$ shell to a $4s$ shell. For example, in a Cu hollow cathode discharge with ~1 Torr Ar carrier gas, the ratio of the Cu ^2D metastable state ($3d^94s^2$) to the ground state ^2S ($3d^{10}4s^1$) was much higher than that measured in a Cu thermal evaporation.[48] Therefore, the population of the manifolds in the Ni $a\,^3D$ state would not likely be appreciably modified by rare-gas collisions and hence the measured Ni density of $a\,^3F_4$ from optical absorption must be multiplied by a factor closer to 4 to obtain the total Ni density.

Figure 4 shows the total number density of Ni atoms which is four times that in the ground state $^3F_4$ (measured by OAS) as a function of rf power on the internal coil, in a continuous-wave Ar plasma. At a fixed pressure, the Ni atom density increases linearly with coil power at low power but tends to saturate at high power. At constant power, the Ni neutral density increases almost linearly with pressure. For example, the Ni density at 20 mTorr is three times that at 8 mTorr for the same power.
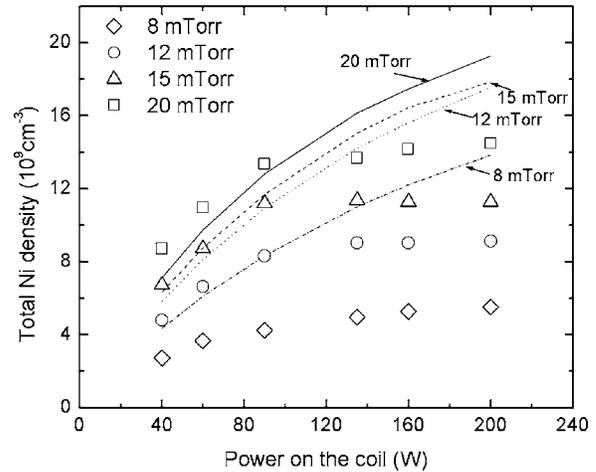
FIG. 4. Symbols: Total Ni densities (four times that of Ni $a\,^3F_4$ state) as a function of coil power and gas pressure (plasma was operated in continuous mode without bias on the target). Ni $a\,^3F_4$ densities were measured using the Ni absorption line at 232.0 nm. Lines: Computed Ni number densities. Squares and solid line: 20 mTorr, triangles and dashed line: 15 mTorr, circles and dotted line: 12 mTorr, and diamonds and dashed-dotted line: 8 mTorr.

2. Calculation of nickel atom number density

Both the power and pressure dependence of the Ni atom density can be understood by applying a Ni mass balance. By assuming that the sputtered Ni neutrals become thermalized by collisions with the background gas, the main loss mechanisms of nickel atoms are diffusion and ionization. The nickel number density is given by

$$n_{\mathrm{Ni}} = \frac{n_S^+ u_B Y_{\mathrm{Ni}} A_{\mathrm{Ni}}/V}{k_{\mathrm{loss}} + k_{\mathrm{iz,Ni}} n_e + k_P n_{\mathrm{Ar}^*}}, \qquad (14)$$

where n_S^+ is the ion (assumed to be Ar$^+$) density at the sheath edge adjacent to the internal coil, equal to $h_R n_0$ (n_0 is the Ar$^+$ density in the plasma center, assumed to be equal to n_e computed above). h_R was estimated to be 0.2 according to the internal coil geometry (diameter=3.5 in.). This estimate might deviate from reality since the Ni coil was the power source of the discharge, which could be different from an inert surface such as the reactor wall. However, this approximation will at least give a conservative estimate of n_S^+ and thus n_{Ni} from Eq. (14). A_{Ni} is the area of Ni surfaces at high negative dc bias exposed to the plasma (in this case only the coil), V is the plasma chamber volume, Y_{Ni} is the sputtering yield of Ni by Ar$^+$, $k_{\mathrm{iz,Ni}}$ is the electron impact ionization rate coefficient for Ni, and k_P is the Penning ionization rate coefficient for Ni by Ar metastables. k_{loss} is the rate coefficient for Ni diffusion to and loss at the walls given by[26,49]

$$1/k_{\mathrm{loss}} = 1/k_D + 1/k_w, \qquad (15)$$

where k_D and k_w are rate coefficients for diffusion and loss at the walls, respectively, given by

$$k_D = \frac{D_{\mathrm{Ni,eff}}}{\Lambda^2}, \qquad (16)$$

$$k_w = \frac{\gamma}{2(2-\gamma)} \frac{\bar{v}_{Ni,Ar} A}{V}. \tag{17}$$

Here, γ is the probability for loss of Ni atoms at the walls (assumed to be unity), $\bar{v}_{Ni,Ar}$ is the reduced mean thermal velocity, and A is the chamber surface area. $D_{Ni,eff}$ is the effective diffusion coefficient of neutral Ni, which is expressed as[29]

$$\frac{1}{D_{Ni,eff}} = \frac{1}{D_{Ni,Ar}} + \frac{1}{D_{Ni,Kn}}, \tag{18}$$

where $D_{Ni,Ar}$ is the binary diffusion coefficient of Ni in Ar gas ($=108$ cm^2 s^{-1} at 1 Torr and 298 K) (Ref. [50]) which was assumed to scale with $T_g^{3/2}$. $D_{Ni,Kn}$ is the Knudsen diffusivity equal to $v_{th} \Lambda / 3$, where $v_{th} = (kT/M)^{1/2}$ is the thermal velocity of Ni atoms having mass M and temperature T.

Most of the sputtered atoms leaving a target were reported to have an energy equal to one-half of the surface binding energy (~ 2.2 eV for Ni) with a Thompson distribution.[51] For Ni atoms, the integrated probability $F(x,p)$ that a sputtered particle thermalizes before traveling a distance x can be expressed in terms of x (in cm) and the background Ar gas pressure p (in mTorr),[52]

$$F(x,p) = \frac{1}{(28/px)^2 + 1}. \tag{19}$$

At high pressures (>100 mTorr), the sputtered Ni atoms would thermalize within a travel distance of 1 cm by collisions with background Ar gas, and their temperature T can be taken to be equal to the measured gas temperature T_g (0.030–0.038 eV). However, at low pressures (<10 mTorr) the Ni temperature would deviate from the gas temperature because the collision mean free path is of the order of the reactor dimension. As a result, a portion of the initial translational energy of Ni ejected from the coil (~ 2.2 eV, half of surface binding energy of Ni) will be retained, resulting in a much higher Ni "temperature." Since the pressure range in this study was 8–20 mTorr, the nonthermalization of sputtered Ni atoms should be included in the calculation of v_{th} and the resultant n_{Ni}. The two extreme temperatures, $T=T_g$ and $T=2.2$ eV, were used to derive the Ni density. The nonthermalization effect was important at 8 mTorr, but not so important at 20 mTorr. For example, for a 200 W plasma at 8 mTorr, the Ni densities calculated using $T=T_g$ and $T=2.2$ eV were 4.25×10^9 and 2.5×10^9 cm^{-3}, correspondingly, while at 20 mTorr the calculated densities were 5.25×10^9 and 4.25×10^9 cm^{-3}, respectively. These differences can be understood from Eq. (18). At higher pressures, $D_{Ni,eff}$ is mainly controlled by $D_{Ni,Ar}$ (which decreases with pressure), and the Ni-temperature-dependent Knudsen diffusion becomes less important. To bracket the uncertainty in the computed Ni number densities introduced by this Ni temperature effect, the values obtained using $T=T_g$ and $T=2.2$ eV were simply averaged to provide the final model predictions.

The self-bias voltage on the internal coil was measured and found to be in the range of 75 ± 10 V for the conditions shown in Fig. 4. This results in a nearly constant Ni sputtering yield of 0.24 at an ion energy of 85 eV (assuming a
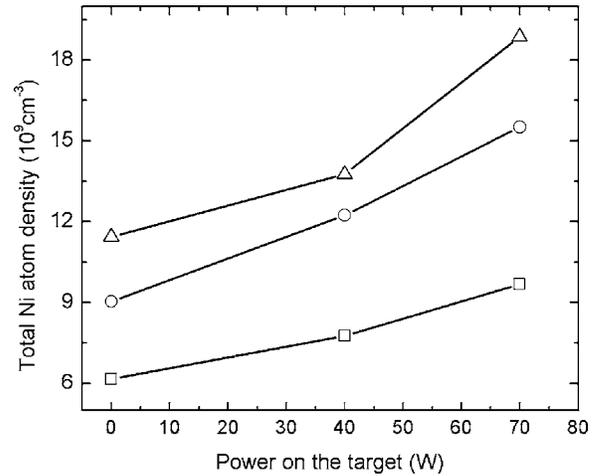
FIG. 5. Total Ni densities (four times that of Ni $a\,^3F_4$ state) as a function of target power and gas pressure (powers both on the coil and on the target were operated in continuous mode). Power on the coil was 200 W. Ni $a\,^3F_4$ densities were measured using the Ni absorption line at 232.0 nm. Squares: 8 mTorr, circles: 15 mTorr, and triangles: 20 mTorr.

nearly constant plasma potential of 10 V).[53] Optical emission measurements (Fig. 3) indicate that the plasma was predominately operated in the inductively coupled mode. Assuming negligible capacitive coupling, the plasma potential variation should be small.

The lines in Fig. 4 are n_{Ni} densities computed from Eq. (14) and the parameters given above. As pressure decreases, the Ni diffusion losses are enhanced. The approximately linear increase in Ni neutral density with a power below 90 W is the result of increased sputtering of the Ni coil, due to the near-linear increase in Ar$^+$ density (the Bohn velocity is nearly independent of power). At higher power, however, Ni diffusion and ionization are enhanced due to the elevated T_g and n_e, resulting in apparent saturation of the Ni neutral density. Of these two Ni loss pathways, diffusion to and loss at the walls account for 65% and electron impact ionization for 35% at 200 W and 20 mTorr.

Model predictions of Ni density agree fairly well with measurements at 20 or 15 mTorr, but lie above the measurements at 8 and 12 mTorr. This discrepancy most likely originates in the conversion of Ni absorption data into absolute Ni number density, where the Ni neutral temperature was assumed to be the gas temperature. In fact, at such low discharge pressures (8 or 12 mTorr) a higher effective Ni temperature would cause Doppler broadening of the Ni absorption line, which would reduce the absorption signals. In other words, with the same Ni absorption percentage, a larger Ni density should be predicted if Doppler broadening was included. For instance, the measured resonant absorption of Ni at 232.0 nm was 7.8% for a plasma at 8 mTorr and 200 W, corresponding to a Ni number density of 5.2×10^9 cm^{-3}, assuming thermalization of Ni with the background gas. If on the other hand, a Ni temperature of 5000 K (0.43 eV) is used, the predicted Ni density would be 1.16×10^{10} cm^{-3}, which is close to the model result (1.38×10^{10} cm^{-3}).

Ni atom densities were also measured as a function of target power (Fig. 5). As the target power increases, the Ni
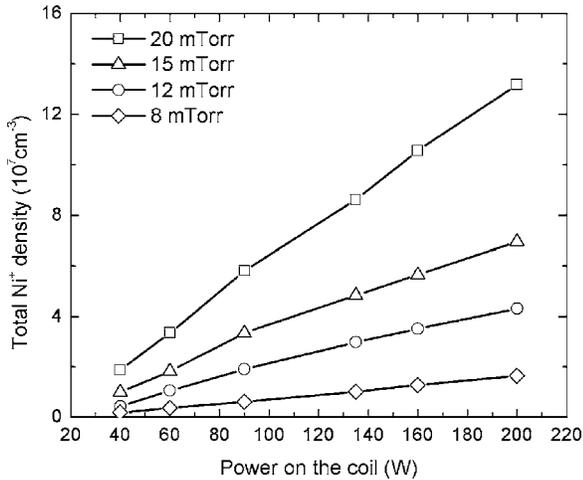
FIG. 6. Calculated Ni$^+$ ion density as a function of coil power and gas pressure (no power on the target). The necessary plasma parameters were derived from a global model, and the Ni density was taken from Fig. 5.

density also increases. The enhancement of Ni density is ~60% when the target power is 70 W (referenced to 0 W), independent of plasma pressure.

E. Nickel positive ion number density

The strong resonant lines connected to the $3d^9$ ($a\,^2D_{5/2}$) ground state of the ion are all in the vacuum ultraviolet and cannot be reached with the present apparatus. However, the 221.6 nm Ni$^+$ line ends in the $3d^84s$ ($a\,^4F_{9/2}$) metastable state lying 8394 cm^{-1} above the ground state. This line has a large oscillator strength ($f = 0.3$) and could be favorable for absorption measurements. Unfortunately, even at the highest plasma power and pressure (e.g., 20 mTorr and 200 W) the resonant absorption rate of the 221.6 nm line was still less than 1%, beyond the limit of our detection (1% absorption on 221.6 nm line would correspond to about 5×10^8 ions/cm^3 in the $a\,^4F_{9/2}$ metastable state).

We can estimate the Ni ion density n_{Ni^+} by a Ni$^+$ mass balance,

$$k_{iz,Ni}n_{Ni}n_e + k_p n_{Ni}n_{Ar^*} = \frac{D_a}{\Lambda^2}n_{Ni^+}, \tag{20}$$

with the Ni$^+$ ambipolar diffusion coefficient D_a given by

$$D_a \approx D_{Ni^+,Ar}\left(1 + \frac{T_e}{T_i}\right), \tag{21}$$

where $D_{Ni^+,Ar}$ is the Ni$^+$ free-diffusion coefficient in Ar, which was roughly assumed to be the same as the Ni neutral diffusion coefficient. T_i is the Ni$^+$ ion temperature and was assumed to be the gas temperature. (This assumption could be suspect at pressures <10 mTorr.[54]) Based on the known values of n_e, T_e, and n_{Ar^*} from the global model, and the value of n_{Ni} estimated by resonant absorption, the Ni$^+$ density n_{Ni^+} was calculated. Contribution of Penning ionization to Ni$^+$ production is likely to be 10–40 times less than that by electron impact ionization, for the same operating condition, assuming a cross section similar to Zn,[55] and Ar metastable densities computed above. The results, presented in Fig. 6, show that the Ni$^+$ density is a strong function of

power on the coil and plasma pressure. Higher power leads to enhanced ion density, and more sputtering, while higher pressure leads to reduced ambipolar diffusion losses of Ni$^+$, increasing the Ni$^+$ ion density.

With a target power of (70 W), the Ni atom density in the plasma was observed to increase by 60% (Fig. 5). Consequently, a 60% enhancement in Ni$^+$ densities is also expected with the assumption that the plasma density and electron temperature are not perturbed by the target power. However, these ion densities would still be one order of magnitude lower than the detection limit by OAS of the 221.6 nm line.

IV. CONCLUSIONS

An inductively coupled argon plasma with a powered internal Ni coil was used to create a nickel-containing discharge with potential applications in ionized physical vapor deposition and nanopantography.[4] An additional Ni target electrode could be powered to further enhance the density of nickel atoms and ions in the discharge. The gas temperature was measured by adding a small amount of N$_2$ and recording the rotationally resolved spectra of the nitrogen second positive system. Fitting to a two-temperature distribution was performed to account for excitation of the N$_2$ C state by argon metastables. Over the range of 8–20 mTorr pressure and 40–200 W coil power, the gas temperature varied between 360 ± 20 and 455 ± 20 K. Optical emission spectroscopy (OES) was used to deduce the relative electron density, while a global model was adopted to compute the absolute electron number density. The Ni atom density measured by optical absorption spectroscopy (OAS) ranged from 2.7×10^9 to 1.5×10^{10} cm^{-3} and was found to increase drastically with plasma pressure. The Ni atom density increased linearly with power at first but approached saturation at high power values. This saturation was attributed to enhanced Ni atom losses due to diffusion (because of increased gas temperature) and electron impact ionization. The computed Ni atom density agreed fairly well with the measurements at 20 and 15 mTorr but was noticeably higher than the measurements at 8 or 12 mTorr. These deviations were most likely due to increased Doppler broadening of the absorbing Ni atoms in the plasma at lower pressures, where a substantial fraction of sputtered Ni atoms remains "hot" due to inefficient Ni thermalization by collisions with rare-gas atoms. The calculated Ni$^+$ ion density was significantly enhanced at higher gas pressure and plasma power. Applying 70 W of power to the Ni target electrode provided a 60% enhancement of the Ni atom density in the plasma. A similar enhancement would be expected for Ni$^+$ ion density assuming that the plasma density and electron temperature were not perturbed by the target power.

[1] International Technology Road Map for Semiconductor (http://www.itrs.net/Common/2005ITRS/Home2005.htm).
[2] S. M. Rossnagel and J. Hopwood, J. Vac. Sci. Technol. B **12**, 449 (1994).

[3]S. M. Rossnagel, J. Vac. Sci. Technol. B **16**, 2585 (1998).

[4]L. Xu, S. C. Vemula, M. Jain, S. K. Nam, V. M. Donnelly, D. J. Economou, and P. Ruchhoeft, Nano Lett. **5**, 2563 (2005).

[5]L. Xu, D. J. Economou, V. M. Donnelly, and P. Ruchhoeft, Appl. Phys. Lett. **87**, 041502 (2005).

[6]Y. Tu, Z. P. Huang, D. Z. Wang, J. G. Wen, and Z. F. Ren, Appl. Phys. Lett. **80**, 4018 (2002).

[7]S. Hofmann, C. Ducati, J. Robertson, and B. Kleisorge, Appl. Phys. Lett. **83**, 135 (2003).

[8]G. S. Duesberg, A. P. Graham, M. Liebau, R. Seidel, E. Unger, F. Kreupl, and W. Hoenlein, Nano Lett. **3**, 257 (2003).

[9]S. M. Rossnagel and J. Hopwood, Appl. Phys. Lett. **63**, 3285 (1993).

[10]C. A. Nichols, S. M. Rossnagel, and S. Hamaguchi, J. Vac. Sci. Technol. B **14**, 3270 (1996).

[11]J. E. Foster, W. Wang, A. E. Wendt, and J. Booske, J. Vac. Sci. Technol. B **16**, 532 (1998).

[12]Y. Andrew, I. Abraham, J. H. Booske, Z. C. Lu, and A. E. Wendt, J. Appl. Phys. **88**, 3208 (2000).

[13]S. Konstantinidis, A. Ricard, M. Ganciu, J. P. Dauchot, C. Ranea, and M. Hecq, J. Appl. Phys. **95**, 2900 (2004).

[14]G. P. Davis and R. A. Gottscho, J. Appl. Phys. **54**, 3080 (1983).

[15]R. A. Porter and W. R. Harshbarger, J. Electrochem. Soc. **126**, 460 (1979).

[16]V. M. Donnelly and M. V. Malyshev, Appl. Phys. Lett. **77**, 2467 (2000).

[17]B. Bai and H. Sawin, J. Vac. Sci. Technol. A **22**, 2014 (2004).

[18]J. Derouard and N. Sadeghi, Chem. Phys. Lett. **102**, 324 (1983).

[19]J. Derouard and N. Sadeghi, Chem. Phys. **88**, 171 (1984).

[20]S. F. Wong and L. Dubé, Phys. Rev. A **17**, 570 (1978).

[21]D. W. Setser, D. H. Stedman, and J. A. Coxon, J. Chem. Phys. **53**, 1004 (1970).

[22]T. D. Nguyen and N. Sadeghi, Chem. Phys. **79**, 41 (1983).

[23]J. Derouard, T. D. Nguyen, and N. Sadeghi, J. Chem. Phys. **72**, 6698 (1980).

[24]S. J. Kang, M.S. thesis, University of Houston, 2005.

[25]N. Sadeghi, M. Cheaib, and D. W. Setser, J. Chem. Phys. **90**, 219 (1989).

[26]M. A. Lieberman and A. J. Lichtenberg, *Principles of Plasma Discharges and Materials Processing*, 2nd ed. (Wiley, New York, 2005).

[27]E. J. McGuire, Phys. Rev. A **20**, 445 (1979).

[28]M. A. Lieberman and S. Ashida, Plasma Sources Sci. Technol. **5**, 145 (1996).

[29]C. Lee and M. A. Lieberman, J. Vac. Sci. Technol. A **13**, 368 (1995).

[30]D. P. Lymberopoulos and D. J. Economou, J. Appl. Phys. **73**, 3668 (1993).

[31]M. V. Malyshev and V. M. Donnelly, Phys. Rev. E **60**, 6016 (1999).

[32]T. Weber, J. B. Boffard, and C. C. Lin, Phys. Rev. A **68**, 032719 (2003).

[33]G. A. Piech, J. B. Boffard, M. F. Gehrke, L. W. Anderson, and C. C. Lin, Phys. Rev. Lett. **81**, 309 (1998).

[34]J. B. Boffard, G. A. Piech, M. F. Gehrke, L. W. Anderson, and C. C. Lin, Phys. Rev. A **59**, 2749 (1999).

[35]B. Ramamurthi and D. J. Economou, Plasma Sources Sci. Technol. **11**, 324 (2002).

[36]P. Subramonium and M. J. Kushner, J. Vac. Sci. Technol. A **20**, 313 (2002).

[37]T. H. Ahn, K. Nakamura, and H. Sugai, Plasma Sources Sci. Technol. **5**, 139 (1996).

[38]M. V. Malyshev and V. M. Donnelly, J. Appl. Phys. **90**, 1130 (2001).

[39]A. C. G. Mitchell and M. W. Zemansky, *Resonance Radiation and Excited Atoms* (Cambridge University Press, London, 1971).

[40]N. Sadeghi *et al.* (unpublished).

[41]G. Nicolussi, W. Husinsky, D. Gruber, and G. Betz, Phys. Rev. B **51**, 8779 (1995).

[42]A. Cortona, W. Husinsky, and G. Betz, Phys. Rev. B **59**, 15495 (1999).

[43]C. He, Z. Postawa, S. W. Rosencrance, R. Chatterjee, B. J. Garrison, and N. Winograd, Phys. Rev. Lett. **75**, 3950 (1995).

[44]E. Vandeweert, V. Philipsen, W. Bouwen, P. Thoen, H. Weidele, R. E. Silverans, and P. Lievens, Phys. Rev. Lett. **78**, 138 (1997).

[45]J. S. Gao, K. Sasaki, H. Toyoda, and H. Sugai, Proceedings of 18th Europhysics Conference on Atomic and Molecular Physics of Ionized Gases (ESCAMPIG), Lecce, Italy, 2006 (unpublished), p. 307.

[46]D. Ohebsian, N. Sadeghi, C. Trassy, and J.-M. Mermet, Opt. Commun. **32**, 81 (1980).

[47]M. Kogelschatz, G. Cunge, and N. Sadeghi, J. Phys. D **37**, 1954 (2004).

[48]P. Baltayan, F. Hartmann, I. Hikmet, and N. Sadeghi, J. Chem. Phys. **97**, 5417 (1992).

[49]P. J. Chantry, J. Appl. Phys. **62**, 1141 (1987).

[50]N. Sadeghi *et al.* (unpublished).

[51]M. W. Thompson, Philos. Mag. **18**, 377 (1968).

[52]A. Gras-Marti and J. A. Valles-Abarca, J. Appl. Phys. **54**, 1071 (1983).

[53]R. V. Stuart and G. K. Wehner, J. Appl. Phys. **33**, 2345 (1962).

[54]H. Matsui, H. Toyoda, and H. Sugai, J. Vac. Sci. Technol. A **23**, 671 (2005).

[55]L. A. Riseberg, W. F. Parks, and L. D. Schearer, Phys. Rev. A **8**, 1962 (1973).